

Spectrometry analysis based on approximation coefficients and deep belief networks

Jian-Ping He¹ · Xiao-Bin Tang^{1,2} · Pin Gong¹ · Peng Wang¹ · Zhen-Yang Han¹ · Wen Yan¹ · Le Gao¹

Received: 28 August 2017/Revised: 12 October 2017/Accepted: 15 November 2017

© Shanghai Institute of Applied Physics, Chinese Academy of Sciences, Chinese Nuclear Society, Science Press China and Springer Nature Singapore Pte Ltd. 2018

Abstract A method of spectrometry analysis based on approximation coefficients and deep belief networks was developed. Detection rate and accurate radionuclide identification distance were used to evaluate the performance of the proposed method in identifying radionuclides. Experimental results show that identification performance was not affected by detection time, number of radionuclides, or detection distance when the minimum detectable activity of a single radionuclide was satisfied. Moreover, the proposed method could accurately predict isotopic compositions from the spectra of moving radionuclides. Thus, the designed method can be used for radiation monitoring instruments that identify radionuclides.

Keywords Approximation coefficient · Deep belief network · Spectrometry analysis · Radionuclide identification · Detection rate

1 Introduction

Distinguishing useful information from irrelevant information is one of the basic concerns of any spectrometric method. However, extracting the correct information from spectral sections is a very complex task for traditional algorithms that identify radionuclides based on peak search because of the limited resolution of the equipment and the often-overlapped peaks [1]. Thus, deconvolution, expert knowledge, and human participation are needed.

An artificial neural network (ANN) is a form of artificial intelligence that attempts to mimic the behavior of the human brain and nervous system [2]. The ANN can extract information using the full spectral range [3]. ANNs have been applied to many aspects of gamma spectral analysis [4–11], and feature extraction is the key step in the majority of these studies. To date, algorithms on radionuclide identification are based on feature extraction, and ANNs are a major technique for performing information extraction. For example, Stinnett et al. [12] proposed a method based on feature extraction and Bayesian classifiers to identify isotopes. Yang et al. [13] developed an algorithm based on feature extraction and feedforward neural networks (NNs) to discriminate alpha–gamma radiation. However, manually supervised feature extraction requires specialized knowledge, and its parameters need to be determined, which is a complex problem.

This work was supported by the National Natural Science Foundation of China (No. 11675078), the Foundation of Graduate Innovation Center in NUAA (No. kfjj20160606, kfjj20170613, and kfjj20170617) and the Fundamental Research Funds for the Central Universities, the Primary Research and Development Plan of Jiangsu Province (No. BE2017729), the Fundamental Research Funds for the Central Universities (No. NJ20160034), the Funding of Jiangsu Innovation Program for Graduate Education (No. KYLX16_0353) and the Fundamental Research Funds for the Central Universities, and the Priority Academic Program Development of Jiangsu Higher Education Institutions.

✉ Xiao-Bin Tang
tangxiaobin@nuaa.edu.cn

¹ Department of Nuclear Science and Engineering, Nanjing University of Aeronautics and Astronautics, Nanjing 210016, China

² Jiangsu Key Laboratory of Nuclear Energy Equipment Materials Engineering, Nanjing 210016, China

Deep learning is a class of machine learning algorithm that uses a cascade of many layers of nonlinear processing units for feature extraction (when the number of hidden layers is smaller than the input dimension), or maps the feature to a higher-dimensional space (when the number of hidden layers is larger than the input dimension), which does not require domain knowledge [14]. This algorithm has been applied to automatic speech recognition, image recognition, smart cars, robots, etc. [15–19]. In this study, an analytical spectrometry method based on approximation coefficients and deep belief networks (DBNs) is proposed. Experiments with different detection times, different numbers of radionuclides, different detection distances, and moving radionuclides were designed to evaluate the identification performance of the proposed method.

2 Theories and methods

2.1 Overview of the proposed method

The proposed method is composed of DBN training and DBN prediction (Fig. 1). The DBN is trained according to the flowchart shown in Fig. 1a. This technique consists of spectrum simulation, extraction of approximation coefficients of the spectrum, and training. First, the model of the related detector is designed, and simulation spectra of the radionuclides of interest are obtained using the Monte

Carlo N-particle transport code (MCNP) (a software package for simulating nuclear processes). Second, approximation coefficients of the spectrum are extracted by wavelet decomposition and normalized to eliminate the intensity difference between different spectra. Then, the normalized approximation coefficients are used as the input to the DBN. Finally, the DBN is trained using the samples of the simulation spectra, which are encoded as the input of the DBN and their target output. For DBN prediction, the trained DBN is used to predict the isotopic composition of the spectrum measured in the real environment using the process shown in Fig. 1b. This process consists of spectral measurement and background subtraction, extraction of the approximation coefficients of the spectrum, and identification. First, radionuclide and background spectra are detected by the detector and smoothed to reduce noise interference. Then, the subtraction spectrum is obtained by subtracting the portion of the smoothed background spectrum according to the ratio of the radionuclide scan time to the background scan time from the smoothed radionuclide spectrum. Second, the approximation coefficients of the subtraction spectrum are extracted by wavelet decomposition and normalized to remove the effect of the change in spectrum intensity. Then, the normalized approximation coefficients are used as the input for the DBN. Finally, the trained DBN is used to predict the isotopic composition of the spectrum measured in the real environment, and the identification performance of the proposed method is

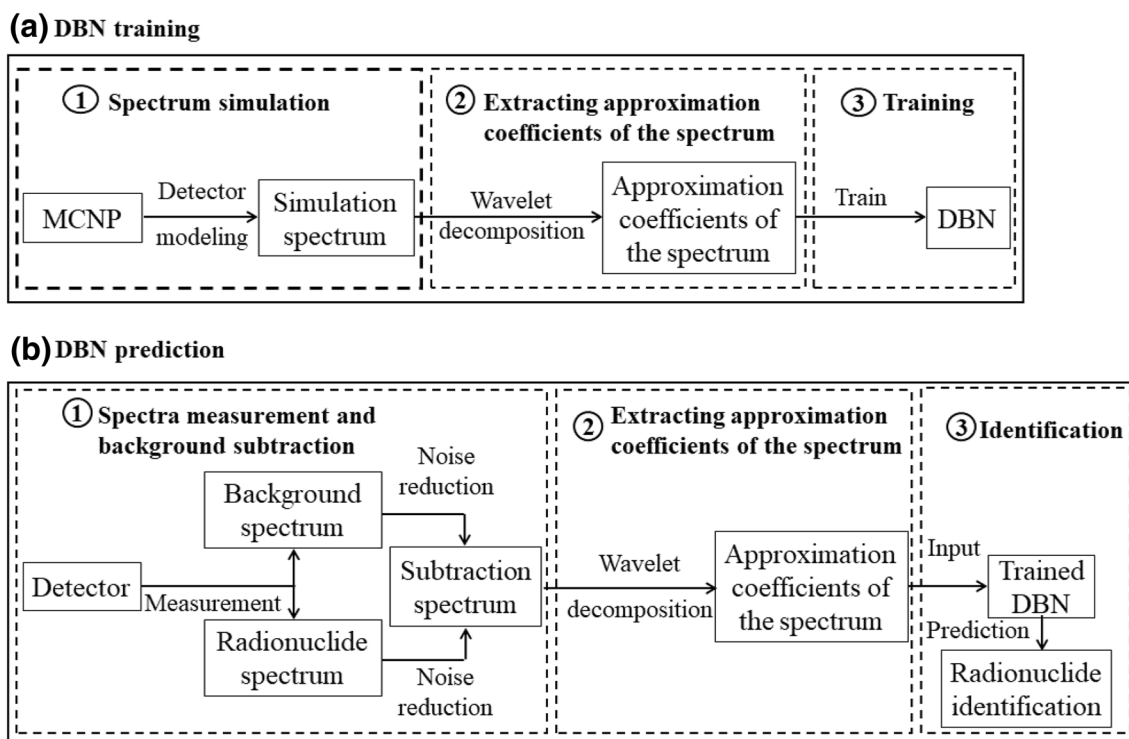


Fig. 1 Schematic diagram of the proposed algorithm

evaluated by comparing the output of the DBN with its target output.

2.2 Approximation coefficients

The low-frequency content is the most important part of many signals, because this component gives the signal its identity. The high-frequency content, on the other hand, imparts flavor, or nuance. Approximations and details are often discussed in wavelet analysis. Approximations are high-scale, low-frequency components of the signal, whereas details are low-scale, high-frequency components. The original signal S would be decomposed into approximations and details after the signal underwent a single-level discrete wavelet transform. This process is accomplished by applying two complementary filters to the original signal, which emerges as two signals, as shown in Fig. 2a.

The decomposition process can be iterated, with successive approximations being decomposed in turn, and the number of iterations is called the decomposition level (Fig. 2b). The $cA_1, cA_2,$ and cA_3 are the approximations of the original signal S , while $cD_1, cD_2,$ and cD_3 are the details at different decomposition levels. Given that the analytical process is iterative, the processes can theoretically be continued indefinitely. In practice, the suitable number of levels is based on the nature of the signal, and a number from 3 to 5 is recommended. Approximation coefficients cA_i ($i = 1, 2, 3, 4, 5$) of the spectrum can be considered as the input to the DBN. The cA_i has the same spectral shape as the original spectrum, but it is more smoothed. The original spectrum (dimension: 1024) detected by an (TI) detector is decomposed in this study by three levels of discrete wavelet transforms (mother wavelet: Daubechies wavelets) using the MATLAB Wavelet Toolbox [20]. The dimension of the extracted approximation coefficients is 128, which is much lower than the dimension of the original spectrum (dimension: 1024). After normalization, the extracted approximation coefficients are used as the input to the DBN.

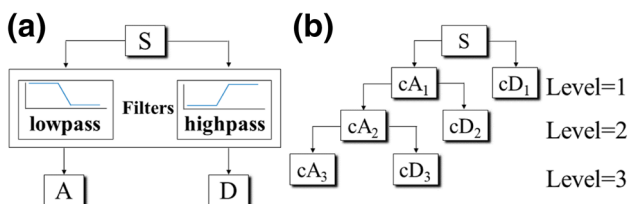


Fig. 2 Schematic of wavelet decomposition. a Single-level and b multilevel discrete wavelet transforms

2.3 DBN model

Deep learning is a machine learning paradigm that focuses on learning deep hierarchical data models. In this algorithm, a hierarchy of intermediate representations is hypothesized to be needed to learn a high-level representation of the data [21]. A DBN is one kind of deep learning. In machine learning, a DBN is a generative graphical model, or alternatively, a type of deep NN composed of multilayers of latent variables (hidden units), with connections between layers but not between units within each layer. A DBN can be viewed as a composition of restricted Boltzmann machines (RBMs), in which the hidden layer of each sub-network serves as the visible layer for the next [22, 23]. Its schematic network structure is shown in Fig. 3. The structure comprises one visible layer, three hidden layers (h^1, h^2, h^3), and one output layer [24]. The number of RBMs is not constant and is determined by the nature of the data. RBMs contain a layer of visible units that represent the data and a layer of hidden units that learn to represent features that capture higher-order correlations in the data. This module is a primitive DBN.

An RBM has only a visible layer and a hidden layer, and these layers are connected by a matrix of symmetrically weighted connections W . No connections are found within a layer. Given a vector of activities v for the visible units, the hidden units are all conditionally independent, facilitating the sampling of a vector h from the factorial posterior distribution over hidden vectors $p(h|v, W)$. Sampling from $p(v|h, W)$ is also easy. A learning signal can be obtained by starting with an observed data vector on the visible units and alternating several times between sampling from $p(h|v, W)$ and $p(v|h, W)$. This signal is simply

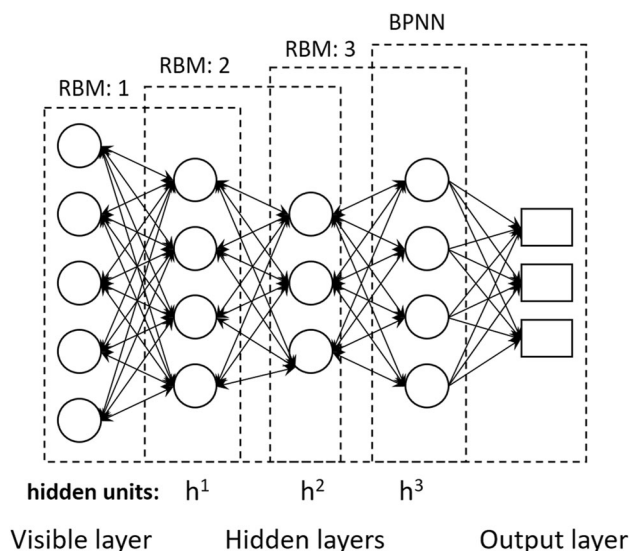


Fig. 3 Schematic overview of a deep belief network (DBN)

the difference between the pairwise correlations of the visible and hidden units at the beginning and end of the sampling. Several reports have provided more detailed descriptions of RBM [25, 26].

The variables of the final hidden layer represent the desired outputs, which can be encoded to the error back-propagation (BP) NN. The BP algorithm functions much better if the feature detectors (hidden units) in the hidden layers are initialized by learning a DBN that models the structure in the input data. The DBN algorithm was realized in this study using a MATLAB Toolbox named DeepLearnToolbox (<https://github.com/rasmusbergpalm/DeepLearnToolbox>), and the key parameters of the DBN used during the training process are as follows: the number of hidden layers is 1, and the dimension of the hidden layer is 1024. The dimension of the visible layer is 128 for extracting 128 approximation coefficients as the input to the DBN, the dimension of the output layer is 9 for selecting the spectra of 9 radionuclides (i.e., ^{57}Co , ^{75}Se , ^{60}Co , ^{133}Ba , ^{137}Cs , ^{192}Ir , ^{241}Am , ^{152}Eu , and ^{238}Pu) as training samples; thus, the established DBN model is $128 \times 1024 \times 9$. Each neuron in the output layer indicated whether the related radionuclide existed or not, and the radionuclide existed in the environment only when the output value of the related output layer neuron was greater than or equal to the threshold (0.85).

3 Experiments and results

The selection of training samples for the DBN is an important part of the proposed method. This process determines the predictive ability of the DBN, so detailed information about training samples will be introduced. Experiments using different detection times, numbers of radionuclides, and detection distances were designed, because these parameters can change the shape of the spectrum. The effect of radionuclides in motion on the identification performance of the proposed method was evaluated, because radionuclides may have a certain velocity in the real environment.

3.1 Assessment method

A gamma-ray spectrometry system, which consists of a $3 \text{ in} \times 3 \text{ in}$ NaI (TI) detector (ORTEC Inc.), a PC-based multichannel analyzer (ORTEC Inc.), and MAESTRO software installed on the PC were used to assess the proposed method, and the MAESTRO 7.01 (ORTEC Inc.) software was used to record the spectra. The energy of this detector ranged from 30 keV to 3000 keV, and the resolution was approximately 7.7% (at 662 keV). The spectra were recorded by sending a request to MAESTRO 7.01

software using its software development kit. Any spectrum that satisfied the requirements could be detected. Table 1 lists the radionuclides utilized in the experiment, and these radionuclides are labeled as Radio-1, Radio-2, and Radio-3.

Given that the DBN can only identify the trained radionuclides, and its predictive ability depends on the number of samples, adding samples of more radionuclides during the training process of the DBN is recommended. However, the majority of radionuclides are not available in the laboratory. Simulation spectra of the radionuclides of interest (i.e., ^{57}Co , ^{75}Se , ^{60}Co , ^{133}Ba , ^{137}Cs , ^{192}Ir , ^{241}Am , ^{152}Eu , and ^{238}Pu) can be obtained by the MCNP, which models the mentioned detector based on its characteristics. All radionuclides except ^{238}Pu are industrial radionuclides. All simulation spectra are broadened with the response function of the mentioned detector.

Detection rate was used to assess the identification performance of the proposed algorithm. This rate is the ratio of the correctly identified data to the total amount of data, as shown in Eq. (1) [27], as follows:

$$\text{Detection rate (\%)} = \frac{\text{TP} + \text{TN}}{\text{TP} + \text{TN} + \text{FP} + \text{FN}} \times 100, \quad (1)$$

where TP indicates true positive, TN indicates true negative, FP indicates false positive, and FN indicates false negative.

The accurate radionuclide identification distance (ARID) of each radionuclide was calculated from the detection rate results with respect to the distance from the source to the detector. The ARID is the maximum distance at which detection rates are reliably ascertained to be above the required level [28]. The detection rate of the acceptance level in this study is 98.3%, as recommended by the ANSI N42.35 standard [29].

3.2 DBN training

Training samples were selected. Simulation spectra of radionuclides of interest (i.e., ^{57}Co , ^{75}Se , ^{60}Co , ^{133}Ba , ^{137}Cs , ^{192}Ir , ^{241}Am , ^{152}Eu , and ^{238}Pu) were simulated by the MCNP, and the normalized simulation spectra generated $511 (2^9 - 1 = 511)$ spectra according to the theory of combinations, which were all used as training samples for

Table 1 Radionuclides for source identification conducted in this study

Label	Radio-1	Radio-2	Radio-3
Radionuclide	^{238}Pu	^{60}Co	^{137}Cs
Activity (μCi)	8.89×10^3	1.59	1.42

the DBN. The conditions with 1 radionuclide corresponded to 9 combinations (i.e., ^{57}Co , ^{75}Se , ^{60}Co , ^{133}Ba , ^{137}Cs , ^{192}Ir , ^{241}Am , ^{152}Eu , and ^{238}Pu), the conditions with 2 radionuclides corresponded to 36 combinations (i.e., $^{57}\text{Co} + ^{75}\text{Se}$, $^{57}\text{Co} + ^{60}\text{Co}$, ..., $^{152}\text{Eu} + ^{238}\text{Pu}$), and the number of combinations for the conditions with 3, 4, 5, 6, 7, 8, and 9 radionuclides can be acquired according to the theory of combinations, which is how we obtained the 511 spectra. The 511 normalized spectra are encoded as the input to the DBN and their target output before DBN training, and the target output was composed of nine figures ranging from 0 to 1. For example, the target output of the ^{57}Co spectrum would be [1 0 0 0 0 0 0 0] if we sequenced the radionuclides as ^{57}Co , ^{75}Se , ^{60}Co , ^{133}Ba , ^{137}Cs , ^{192}Ir , ^{241}Am , ^{152}Eu , and ^{238}Pu . So, the target output of the ^{75}Se spectrum was [0 1 0 0 0 0 0 0], the target output of the $^{57}\text{Co} + ^{75}\text{Se}$ spectrum was [1 1 0 0 0 0 0 0], and so on.

Whether the trained DBN has learned the training samples properly should be verified. If not, the related parameters (section: DBN model) of the DBN should be adjusted until the mean square error of the DBN on the training set reaches an acceptable value. Table 2 lists the results of the DBN training. The trained DBN learned the high-level features of the training set completely. Theoretically, this DBN could predict the isotopic compositions of the spectrum measured in the real environment for all radionuclides (i.e., ^{57}Co , ^{75}Se , ^{60}Co , ^{133}Ba , ^{137}Cs , ^{192}Ir , ^{241}Am , ^{152}Eu , and ^{238}Pu) with a detection rate of 100%.

3.3 Effect of detection time on the proposed method

Experiments using different detection times were conducted, because detection time can lead to a change in spectral intensity. The detector was installed at a fixed location, and the radionuclides were placed in front of the detector at point A (Fig. 4). The background spectrum without any source was recorded for 300 s to generate the background template. The spectra of Radio-1, Radio-2, and Radio-3 placed at point A (Fig. 4) were recorded to evaluate the detection time effect on the identification performance of the proposed method. The measurement was repeated 10 times for each condition, and detection times



Fig. 4 (Color online) Sketch of the first experimental environment

were 1, 2, 3, 4, and 5 s. For example, the measurement for Radio-1 with monitoring point at A (Fig. 4) and a detection time of 1 s would be repeated 10 times. The same rules apply to other detection times and radionuclides. A total of 150 spectra were recorded, which were all used as verifying samples. Ten spectra could be recorded at each detection time for each radionuclide, resulting in 50 spectra for each radionuclide. Each spectrum has a sample number, the value of which was determined by the measurement sequence. For example, 10 Radio-1 spectra with a detection time of 1 s would have sample numbers 1–10, 10 Radio-1 spectra with a detection time of 2 s would have sample numbers 11–20, etc. The same rules apply to Radio-2 and Radio-3.

We focused only on the output neurons of the DBN for ^{238}Pu , ^{60}Co , and ^{137}Cs to select three radionuclides (^{238}Pu , ^{60}Co , and ^{137}Cs) to evaluate the identification performance of the proposed method in the real environment, and all the results related to verifying samples in this study were computed by analyzing the output value of the above three output neurons. Figure 5 shows the results for samples with different detection times when only ^{238}Pu exists in the environment. The output value of the DBN for ^{238}Pu is greater than the threshold (0.85) at different times when only ^{238}Pu exists in the environment. The output value for

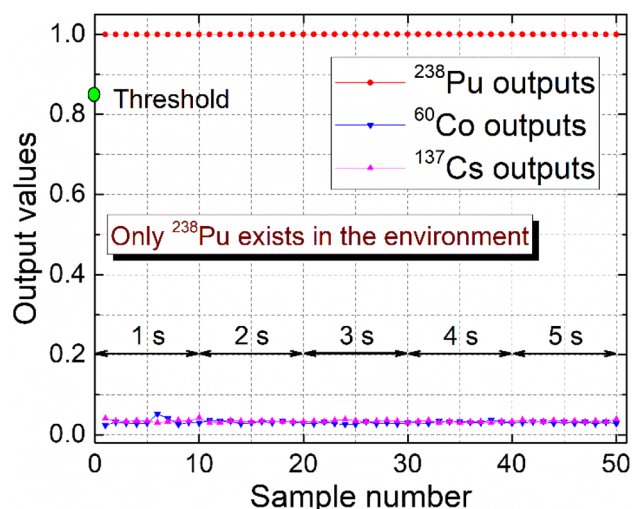


Fig. 5 (Color online) Output values of deep belief network (DBN) at different sample numbers when only ^{238}Pu exists in the environment

Table 2 Results of DBN training

Radionuclide	^{57}Co	^{75}Se	^{60}Co	^{133}Ba	^{137}Cs
Detection rate (%)	100	100	100	100	100
Radionuclide	^{192}Ir	^{241}Am	^{152}Eu	^{238}Pu	
Detection rate (%)	100	100	100	100	

^{60}Co or ^{137}Cs is less than the threshold, indicating the presence of ^{238}Pu in the environment, but the absence of ^{60}Co and ^{137}Cs . The results are consistent with the actual situation because of the normalization of approximation coefficients, which can eliminate the effect of the change in spectral intensity. Therefore, the identification performance of the proposed method is not affected by the detection time if the minimum net count of the spectrum of related radionuclides is satisfied. Figures 6 and 7 illustrate similar results. The net count of the spectrum of each radionuclide measured at point A (Fig. 4) with a detection time of 5 s, and the count of background spectrum with a detection time of 5 s are listed in Table 3. The dose rate of the background without a shielding apparatus was measured in the laboratory (approximately $0.1 \mu\text{Sv/h}$).

3.4 Effect of the number of radionuclides on the proposed method

Experiments with different numbers of radionuclides were performed, because this parameter can change the spectral shape. The detector was installed at a fixed location, and the radionuclides were placed in front of the detector at point A (Fig. 4). The spectra of the cases with different numbers of radionuclides (i.e., Radio-1, Radio-2, Radio-3, Radio-1 + Radio-2, Radio-1 + Radio-3, Radio-2 + Radio-3, and Radio-1 + Radio-2 + Radio-3) placed at point A (Fig. 4) were recorded to evaluate the effect of the number of radionuclides on the identification performance of the proposed method. The measurement was repeated 10 times for each condition, and the detection time was 5 s. For example, the measurement for Radio-1 with monitoring point at A (Fig. 4) and a detection time of 5 s would be repeated 10 times. The same rules apply to

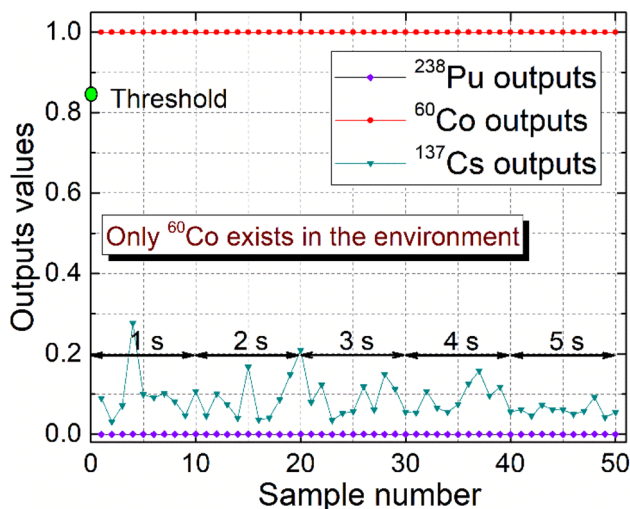


Fig. 6 (Color online) Output values of DBN at different sample numbers when only ^{60}Co exists in the environment

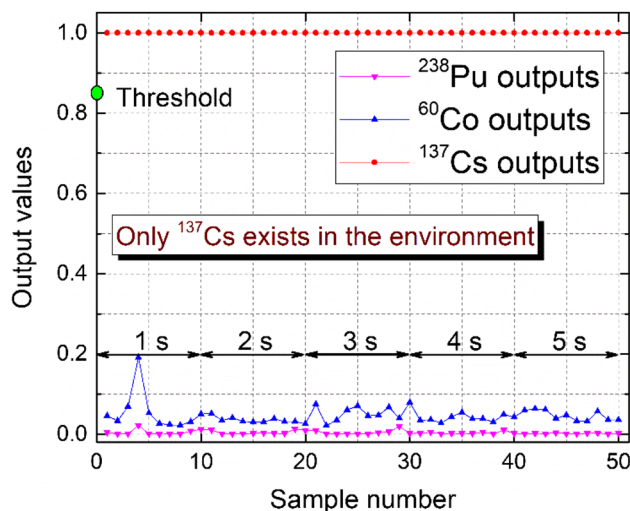


Fig. 7 (Color online) Output values of DBN at different sample numbers when only ^{137}Cs exists in the environment

Table 3 Count of radionuclides and background spectrum with a detection time of 5 s

Radionuclide	^{238}Pu	^{60}Co	^{137}Cs
Net count	3049	8161	3585
Background	2614	2614	2614

other combinations. Hence, 70 spectra were recorded, which were all used as verifying samples. Three combinations (i.e., Radio-1, Radio-2, and Radio-3) correspond to the condition with 1 radionuclide. Three combinations (i.e., Radio-1 + Radio-2, Radio-1 + Radio-3, and Radio-2 + Radio-3) correspond to the condition with two radionuclides. One combination (i.e., Radio-1 + Radio-2 + Radio-3) corresponds to the condition with three radionuclides.

Table 4 lists the results of samples with different numbers of radionuclides. All radionuclides (i.e., ^{238}Pu , ^{60}Co , and ^{137}Cs) have a detection rate of 100%, which demonstrates that the proposed algorithm can predict the isotopic compositions of the spectra of multiple radionuclides. This phenomenon is due to the fact that the DBN was trained using samples with mixed spectra of multiple radionuclides. However, the training samples are composed of simulation spectra which differ from the spectra measured in the real environment, especially in the low-energy

Table 4 Single radionuclide detection rates (%) of the samples with different numbers of radionuclides

Number	^{238}Pu	^{60}Co	^{137}Cs
1	100	100	100
2	100	100	100
3	100	100	100

region, although their shapes are similar. This phenomenon may reflect the fact that the DBN has strong tolerance, indicating promising machine learning for spectrometry analysis.

3.5 Effect of detection distance on the proposed method

Experiments with different detection distances were conducted, because this parameter can also lead to a change in the spectral shape. The detector was installed at a fixed location, and the radionuclides were placed in front of the detector at points A, B, ..., O (15 points) at 10-cm intervals (Fig. 8). The spectra of the radionuclides were recorded to evaluate the effect of detection distance on the identification performance of the proposed method. The measurement was repeated 10 times for each condition, and the detection time was 10 s. For example, the measurement for Radio-1 with monitoring point at A (Fig. 8) and a detection time of 10 s would be repeated 10 times. The same rules apply to other monitoring points or radionuclides. Thus, 450 spectra were recorded, which were all used as verifying samples.

Figure 9 shows the results of samples with different detection distances. The ARIDs of Radio-1 (^{238}Pu with an activity of $8.89 \times 10^3 \mu\text{Ci}$ and a detection time of 10 s), Radio-2 (^{60}Co with an activity of $1.59 \mu\text{Ci}$ and a detection time of 10 s), and Radio-3 (^{137}Cs with an activity of $1.42 \mu\text{Ci}$ and a detection time of 10 s) are greater than or equal to 60, 70, and 60 cm, respectively. The corresponding minimum detectable activities (MDAs) of Radio-1 (^{238}Pu with a detection distance of 60 cm and a detection time of 10 s), Radio-2 (^{60}Co with a detection distance of 70 cm and a detection time of 10 s), and Radio-3 (^{137}Cs with a detection distance of 60 cm and a detection time of 10 s) are less than or equal to 8.89×10^3 , 1.59, and $1.42 \mu\text{Ci}$, respectively [30, 31]. Thus, the identification performance of the proposed method is not affected by the detection distance under certain conditions, because the effect of detection distance on the proposed method can be eliminated by the normalization of approximation coefficients. The detection rate of radionuclides (i.e., ^{238}Pu , ^{60}Co , and ^{137}Cs) is over 60% when the detection distance is greater than the ARID of the related radionuclide (Fig. 9a–c). This result is due to the fact that the detection rate is a statistic, and the numerator TN of Eq. (1) remains almost

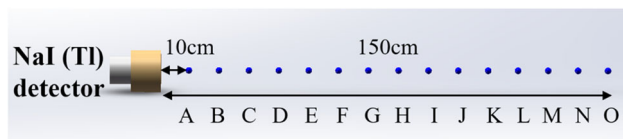


Fig. 8 (Color online) Sketch of the second experimental environment

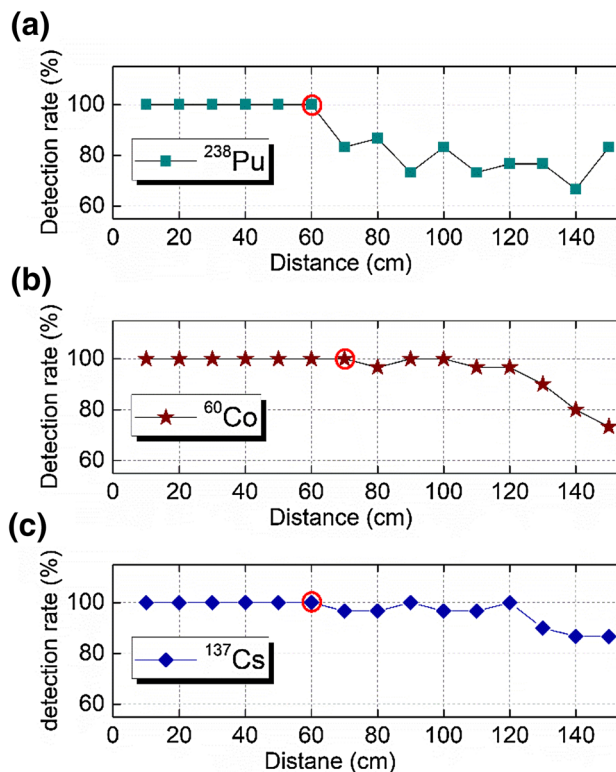


Fig. 9 (Color online) Single radionuclide detection rates (%) of samples with different detection distances: **a** ^{238}Pu , **b** ^{60}Co , and **c** ^{137}Cs

constant, although the numerator TP in Eq. (1) decreases with an increase in distance. This phenomenon is due to the low percentage of error in identification, which indicates the proposed method is a robust method.

The spectra of radionuclides (^{238}Pu , ^{60}Co , and ^{137}Cs) placed in front of the detector according to their ARIDs are plotted to further visualize the identification performance of the proposed method (Fig. 10). The signal-to-noise ratio (SNR) is extremely low in this condition, and the corresponding characteristic peaks of radionuclides are not obvious (fewer counts in the photopeak region). However, the proposed method can recognize these radionuclides with a detection rate of 100%. Therefore, the proposed method is suitable for fast radionuclide identification, because it requires a lower spectrum count.

3.6 Effect of radionuclides in motion on the proposed method

Radionuclides may be carried by people or transported by car in the real environment. Thus, these molecules have a certain velocity. The effect of radionuclides in motion on the identification performance of the proposed method should be evaluated. The detector was installed at a fixed location, and the radionuclides were placed in front of the

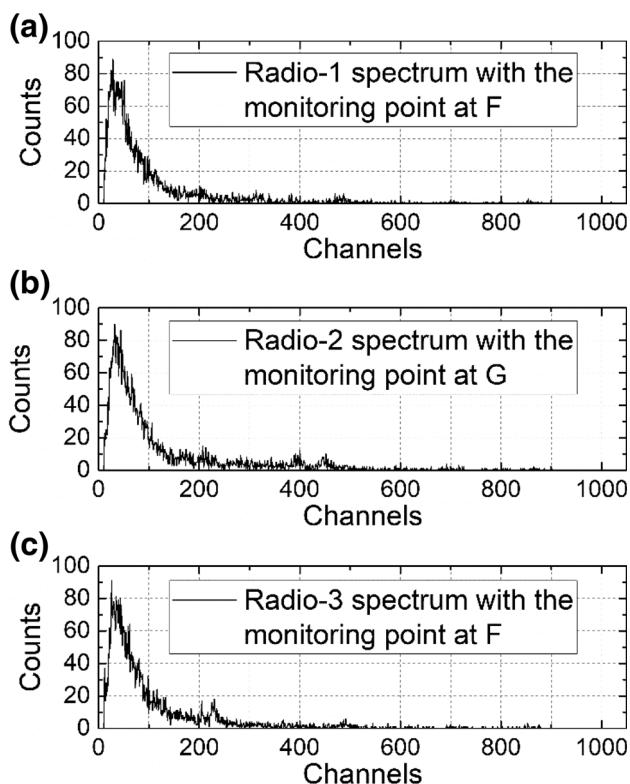


Fig. 10 Spectra of radionuclides with the monitoring point at their ARIDs: **a** Radio-1, **b** Radio-2, and **c** Radio-3

detector at points A, B, ..., O at 10-cm intervals (Fig. 8). An experiment was designed to assess the effect of radionuclides in motion on the identification performance of the proposed method. A person with Radio-1, Radio-2, and Radio-3 approached point A from the starting point O along the line segment OA at a speed of approximately 0.375 m/s. The whole process took approximately 4 s, and 33 spectra were recorded at intervals of approximately 0.1 s. All spectra were used as verifying samples.

Figure 11 shows the results of the samples of the moving radionuclides. The output value of the DBN for ^{137}Cs is greater than the threshold (0.85) at time 2.5 s, indicating the identification of ^{137}Cs . The corresponding value for ^{238}Pu is also greater than the threshold (0.85) at time 2.76 s, indicating the identification of ^{238}Pu . The corresponding value for ^{60}Co is greater than the threshold (0.85) at time 3.0 s, indicating the identification of ^{60}Co . Thus, the output value of the DBN for related radionuclides is always beyond the threshold after the corresponding radionuclide is recognized. The proposed method exhibits enhanced identification performance for the spectra of moving radionuclides and requires only a short time to identify all radionuclides in the environment. This characteristic is recommended for fast radionuclide identification.

Figure 12 demonstrates the spectra in radionuclide identification. The spectrum has a low SNR at each time of

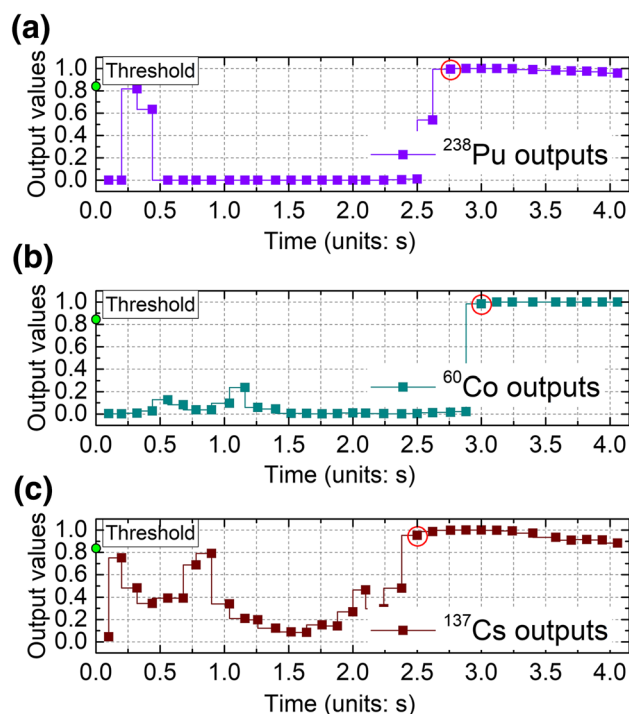


Fig. 11 (Color online) Output values of DBN for samples of moving radionuclides at different times. Output channels of DBN for **a** ^{238}Pu , **b** ^{60}Co , and **c** ^{137}Cs

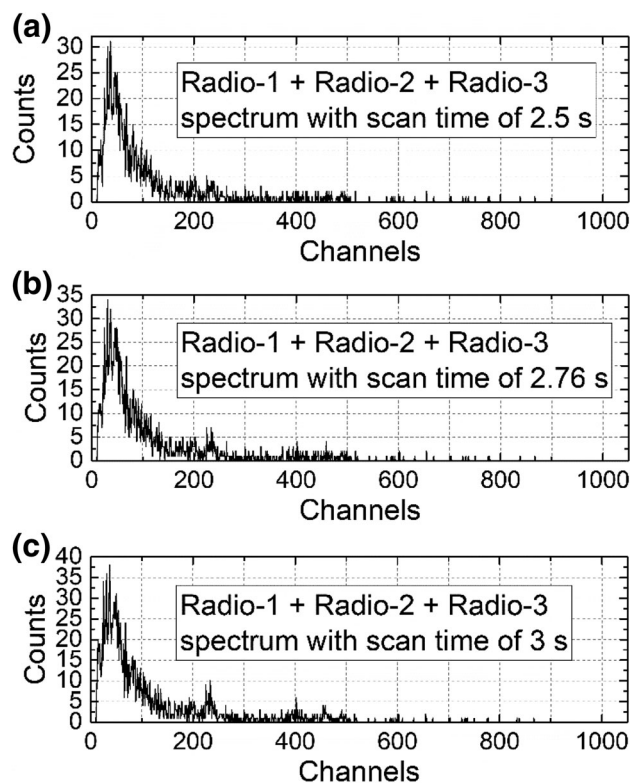


Fig. 12 Spectra of radionuclides (i.e., Radio-1 + Radio-2 + Radio-3) at their time of identification. **a** $t = 2.5$ s, **b** $t = 2.76$ s, and **c** $t = 3.0$ s

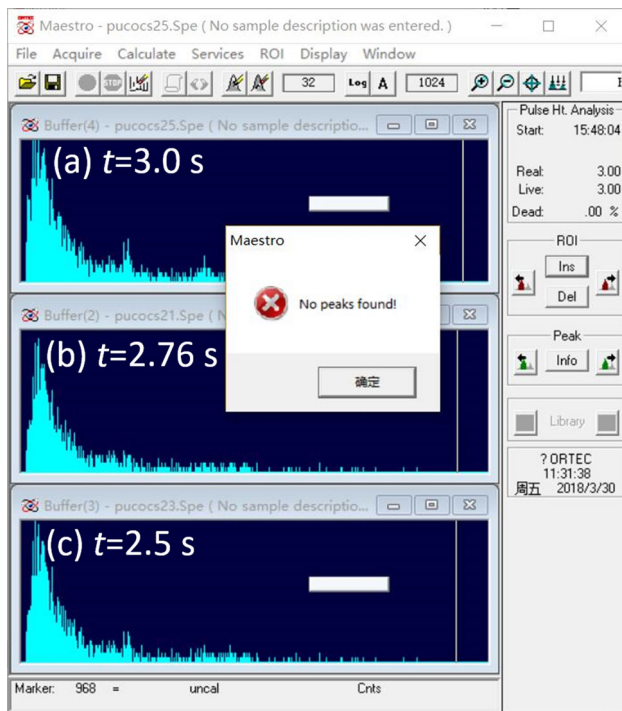


Fig. 13 (Color online) Identification results of MAESTRO 7.01 software for spectra of radionuclides (i.e., Radio-1 + Radio-2 + Radio-3) at the times of **a** $t = 2.5$ s, **b** $t = 2.76$ s, and **c** $t = 3.0$ s

identification of the related radionuclide, and its corresponding characteristic peak cannot be observed. The proposed method is not based on peak detection, but on information from the full spectrum. The proposed algorithm makes a judgment using information from the full spectrum, contrary to the method based on peak detection. Specialized knowledge, deconvolution, and other parameters previously used were not needed after the DBN was trained.

The identification results of the spectra contained within Fig. 12a–c using MAESTRO 7.01 software (a software for gamma-ray spectrometry analysis) were all “No peaks found,” as shown in Fig. 13. This is primarily because there were lower counts of radionuclide spectrum in the photopeak region, so the MAESTRO 7.01 software could not find a peak that satisfied its default requirement. Experimental results demonstrate once again that the proposed method is not based on peak detection, but on information from the full spectrum.

4 Conclusion

A method of spectrometry analysis based on approximation coefficients and a DBN was proposed in this study. This method consisted of DBN training and DBN prediction. Approximation coefficients of the spectrum were extracted

by wavelet decomposition. The DBN was trained using samples of simulation spectra of radionuclides of interest and was used to predict the isotopic compositions of the spectrum measured in the real environment. Experimental results show that the identification performance of the proposed method was not affected by the detection time, number of radionuclides, or detection distance when the MDA of a single radionuclide was satisfied. The radionuclides used in this study were ^{238}Pu ($8.89 \times 10^3 \mu\text{Ci}$), ^{60}Co ($1.59 \mu\text{Ci}$), and ^{137}Cs ($1.42 \mu\text{Ci}$). The dose rate of the background without a shielding apparatus was measured in the laboratory (approximately $0.1 \mu\text{Sv/h}$). The proposed method showed better performance for predicting the isotopic compositions of the spectrum of moving radionuclides. The proposed method identified the isotopic compositions in the spectrum using information from the full spectrum, contrary to the method based on peak detection.

The proposed method may exhibit enhanced identification performance for the spectrum of radionuclides with higher energy, because the DBN is trained using samples of the simulation spectra of radionuclides of interest, and the difference between the spectrum simulated by the MCNP and that measured in the real environment in the low-energy (< 100 keV) region is larger. In summary, a novel method for spectrometry analysis was developed which overcomes the difficulties caused by the insufficient availability of the majority of radionuclides in the laboratory. Further work, such as using different detectors (e.g., lanthanum bromide scintillation detector, cadmium zinc telluride detector, high-purity germanium detector), and the addition of gamma-ray shielding will be performed to verify the identification performance of the proposed method. In addition, complex methods combined with the latest advanced algorithms, such as optimization algorithms (e.g., genetic algorithms, particle swarm algorithms), feature extraction algorithms (Karhunen–Loeve transform, singular-value decomposition), and fuzzy logic algorithms, will be studied to develop more intelligent methods for spectrometry analysis. The proposed method can be executed in a mobile or an embedded system because of the simplicity of the trained DBN. In this study, the algorithm was executed on a Windows-based mini-PC. The proposed method may potentially be suitable for radionuclide identification of radiation monitoring instruments because of its high stability and low execution time.

References

1. M. Morháč, V. Matoušek, Complete positive deconvolution of spectrometric data. *Digit. Signal Process.* **19**, 372–392 (2009). <https://doi.org/10.1016/j.dsp.2008.06.002>

2. L.J. Kangas, P.E. Keller, E.R. Siciliano et al., The use of artificial neural networks in PVT-based radiation portal monitors. *Nucl. Instrum. Methods Phys. Res. A* **587**, 398–412 (2008). <https://doi.org/10.1016/j.nima.2008.01.065>
3. L. Chen, Y.X. Wei, Nuclide identification algorithm based on K–L transform and neural networks. *Nucl. Instrum. Methods Phys. Res. A* **598**, 450–453 (2009). <https://doi.org/10.1016/j.nima.2008.09.035>
4. C. Bobin, O. Bichler, V. Lourenco et al., Real-time radionuclide identification in γ -emitter mixtures based on spiking neural network. *Appl. Radiat. Isot.* **109**, 405–409 (2016). <https://doi.org/10.1016/j.apradiso.2015.12.029>
5. H. Hata, K. Yokoyama, Y. Ishimori et al., Application of support vector machine to rapid classification of uranium waste drums using low-resolution γ -ray spectra. *Appl. Radiat. Isot.* **104**, 143–146 (2015). <https://doi.org/10.1016/j.apradiso.2015.06.030>
6. M.E. Medhat, Artificial intelligence methods applied for quantitative analysis of natural radioactive sources. *Ann. Nucl. Energy* **45**, 73–79 (2012). <https://doi.org/10.1016/j.anucene.2012.02.013>
7. S. Dragović, A. Onjia, G. Bačić, Simplex optimization of artificial neural networks for the prediction of minimum detectable activity in gamma-ray spectrometry. *Nucl. Instrum. Methods Phys. Res. A* **564**, 308–314 (2006). <https://doi.org/10.1016/j.nima.2006.03.047>
8. S. Dragović, A. Onjia, S. Stanković et al., Artificial neural network modelling of uncertainty in gamma-ray spectrometry. *Nucl. Instrum. Methods Phys. Res. A* **540**, 455–463 (2005). <https://doi.org/10.1016/j.nima.2004.11.045>
9. S. Dragović, A. Onjia, Prediction of peak-to-background ratio in gamma-ray spectrometry using simplex optimized artificial neural network. *Appl. Radiat. Isot.* **63**, 363–366 (2005). <https://doi.org/10.1016/j.apradiso.2005.03.009>
10. V. Pilato, F. Tola, J.M. Martinez et al., Application of neural networks to quantitative spectrometry analysis. *Nucl. Instrum. Methods Phys. Res. A* **422**, 423–427 (1999). [https://doi.org/10.1016/S0168-9002\(98\)01110-3](https://doi.org/10.1016/S0168-9002(98)01110-3)
11. P. Olmos, J.C. Diaz, J.M. Perez et al., Application of neural network techniques in gamma spectroscopy. *Nucl. Instrum. Methods Phys. Res. A* **312**, 167–173 (1992). [https://doi.org/10.1016/0168-9002\(92\)90148-W](https://doi.org/10.1016/0168-9002(92)90148-W)
12. J. Stinnett, M. Watson, C.J. Sullivan et al., Uncertainty analysis of wavelet-based feature extraction for isotope identification on NaI gamma-ray spectra. *IEEE Trans. Nucl. Sci.* (2017). <https://doi.org/10.1109/TNS.2017.2676045>
13. C.F. Yang, C.Q. Feng, W.H. Dong et al., Alpha-gamma discrimination in BaF₂ using FPGA-based feedforward neural network. *IEEE Trans. Nucl. Sci.* (2017). <https://doi.org/10.1109/TNS.2017.2691729>
14. L. Deng, D. Yu, Deep learning: methods and applications. *Found. Trends Signal Process.* **7**, 197–387 (2014). <https://doi.org/10.1561/20000000039>
15. Đ.T. Grozdić, S.T. Jovičić, M. Subotić, Whispered speech recognition using deep denoising autoencoder. *Eng. Appl. Artif. Intell.* **59**, 15–22 (2017). <https://doi.org/10.1016/j.engappai.2016.12.012>
16. B. Bermeitinger, A. Freitas, S. Doing et al., *Object Classification in Images of Neoclassical Furniture Using Deep Learning*, vol. 482 (Springer, Berlin, 2016), pp. 109–112. https://doi.org/10.1007/978-3-319-46224-0_10
17. J. Stilgoe, Machine learning, social learning and the governance of self-driving cars. *SSRN Electron. J.* (2017). <https://doi.org/10.2139/ssrn.2937316>
18. D. Ribeiro, A. Mateus, J.C. Nascimento et al., A real-time deep learning pedestrian detector for robot navigation. Paper presented at the 2017 IEEE international conference on autonomous robot system and competitions (ICARSC), Coimbra, pp. 165–171, April 2017
19. D. Ravi, C. Wong, B. Lo et al., A deep learning approach to on-node sensor data analytics for mobile or wearable devices. *IEEE J. Biomed. Health Inform.* **21**, 56–64 (2017). <https://doi.org/10.1109/JBHI.2016.2633287>
20. M. Misiti, Y. Misiti, G. Oppenheim et al., *Wavelet Toolbox for Use with Matlab*, 1st edn. (The Matworks Inc, Natick, 1996), pp. 38–41
21. Y. Bengio, Learning deep architectures for AI. *Found. Trends Mach. Learn.* **2**, 1–127 (2009). <https://doi.org/10.1561/22000000006>
22. G.E. Hinton, R.R. Salakhutdinov, Reducing the dimensionality of data with neural networks. *Science* **313**, 504–507 (2006). <https://doi.org/10.1126/science.1127647>
23. G.E. Hinton, S. Osindero, Y.W. Teh, A fast learning algorithm for deep belief nets. *Neural Comput.* **18**, 1527–1554 (2006). <https://doi.org/10.1162/neco.2006.18.7.1527>
24. R.B. Palm, Prediction as a candidate for learning deep hierarchical models of data. *Found. Trends Mach. Learn.* **5**, 1–127 (2012). <https://doi.org/10.1561/22000000006>
25. A. Fischer, C. Igel, An introduction to restricted Boltzmann machines, in *Progress in Pattern Recognition, Image Analysis, Computer Vision, and Applications*, vol. 7441, pp. 14–36 (2012). https://doi.org/10.1007/978-3-642-33275-3_2
26. G. Hinton, Practical guide to training restricted Boltzmann machines. *Momentum* **9**, 599–619 (2012). https://doi.org/10.1007/978-3-642-35289-8_32
27. E. Min, M. Ko, Y. Kim et al. A peak detection in noisy spectrum using principal component analysis, in *Nuclear science symposium and medical imaging conference (NSS/MIC)*. 2012 IEEE, pp. 62–65 (2012). <https://doi.org/10.1109/nssmic.2012.6551061>
28. E. Min, M. Ko, H. Lee et al., Identification of radionuclides for the spectroscopic radiation portal monitor for pedestrian screening under a low signal-to-noise ratio condition. *Nucl. Instrum. Methods Phys. Res. A* **758**, 62–68 (2014). <https://doi.org/10.1016/j.nima.2014.05.021>
29. N. Ansi, American national standard for evaluation and performance of radiation detection portal monitors for use in homeland security. *IEEE* **c1-35**, 1–38 (2004). <https://doi.org/10.1109/ieeestd.2004.94428>
30. X.B. Tang, J. Meng, P. Wang et al., Simulated minimum detectable activity concentration (MDAC) for a real-time UAV airborne radioactivity monitoring system with HPGe and LaBr 3 detectors. *Radiat. Meas.* **85**, 126–133 (2016). <https://doi.org/10.1016/j.radmeas.2015.12.031>
31. C.H. Gong, G.Q. Zeng, L.Q. Ge et al., Minimum detectable activity for NaI(Tl) airborne γ -ray spectrometry based on Monte Carlo simulation. *Sci. China Technol. Sci.* **57**, 1840–1845 (2014). <https://doi.org/10.1007/s11431-014-5553-x>